Eur. J. Mineral.
2001, **13**, 311-318

Dedicated to Prof. Dr. Wolfgang F. Müller
on the occasion of his 60th birthday

TEM study of a chromium-bearing kyanite from a mantle xenolith: Evidence for an alumina-rich exsolution precursor phase

RICHARD WIRTH[1,*], KLAUS LANGER[2] and ALEXEJ N. PLATONOV[3]

[1] GeoForschungsZentrum Potsdam, Telegrafenberg C120, D-14473 Potsdam, Germany
[2] Institut für Angewandte Geowissenschaften I, Technische Universität, D-10623 Berlin, Germany
[3] Institute of Geochemistry, Mineralogy and Ore Formation, Academy of Sciences of Ukraine, 252680 Kyiv, Ukraine

Abstract: The chromium-bearing kyanite specimen U-158, extracted from a kyanite-eclogite xenolith in a Yakutian kimberlite pipe was studied by transmission electron microscopy TEM. This specimen has an analysed composition $(Al_{1.989}\ Cr_{0.014}\ Fe_{0.007}\ Ti_{0.001})_{\Sigma=2.011}\ [O/Si_{0.990}O_4]$ and has been examined by electronic absorption and fluorescence spectroscopy (Platonov *et al*., 1998).

The (010) oriented foil previously studied by spectroscopy, shows areas of dark diffraction contrast which were found to originate from incipient alumina-type exsolutions forming platelets about 2 nm thick and 5-10 nm wide. They are intergrown with the kyanite matrix and have the orientation relationships $[0\bar{1}\bar{1}]_{ky}$ // $[01\bar{1}0]_{cor}$ and $(100)_{ky}$ // $(0001)_{cor}$. The volume fraction of these exsolution precursors is estimated to be less than 0.1 vol. %. Elemental mapping using inelastically scattered electrons in the EELS spectra (Al-L_3 and Si-L_3 edges) demonstrated Si-depletion and Al-enrichment in the exsolution precursors. Furthermore, EDX analysis with a nominal spot size of 4 nm confirmed the areas with dark contrasts to be more Al-rich than the kyanite matrix without these contrasts, while chromium contents were the same. The EDX analysis is evidently a superposition of the chemical composition of both the kyanite matrix and the additional phase identified by TEM. In any case, the chemical analysis confirms the crystallographic inferences about composition.

The results confirm the presence of a precursor of an Al-rich, chromium-bearing corundum-type exsolution as previously suggested to explain two greatly differing crystal fields for Cr^{3+} in the studied chromium-bearing kyanite.

Key-words: TEM, HRTEM, kyanite, precursor of corundum, exsolution.

Introduction

In a recent spectroscopic study of chromium-bearing kyanites (Platonov *et al*., 1998), the electronic absorption and luminescence results showed chromium (III) to be present in two greatly different crystal fields a and b, giving rise to two sets of bands derived from the well known dd-transitions of octahedral Cr^{3+}, $^4A_{2g} \rightarrow {}^4T_{2g}$ and $\rightarrow {}^4T_{1g}$. The crystal field parameters 10Dq and B derived from sets a or b were found to differ so greatly from each other that an allocation of chromium in the different octahedral sites of the kyanite structure (Burnham, 1963; Winter & Ghose, 1979) could not account for this effect. Indeed, in the case of environment a, the parameters are those typical of chromium substituting for aluminium in silicates without constitutional OH^- but with $(Al\text{-}O)^{[6]}$ – distances similar to those in kyanite, as sapphirine, some mantle garnets or beryl. On the other hand, the parameters for Cr^{3+} in environment b closely resemble those typical for chromium in oxide matrices such as corundum or spinel. Therefore, it has been proposed that a fraction of the total chromium content "....corresponding to chromium type b is substituting for octahedral aluminium in an Al-bearing oxide matrix which may occur as a precursor phase of an

*e-mail:wirth@gfz-potsdam.de

DOI: 10.1127/0935-1221/01/0013-0311

0935-1221/01/0013-0311 $ 2.00

exsolving corundum type solid solution in the kyanite studied." (Platonov *et al*., 1998).

This hypothesis is best checked by a TEM and HRTEM investigation. The present paper reports the results of such a study. The results support the above hypothesis and explain the two greatly different crystallographic environments a and b found spectroscopically in chromium-bearing kyanites.

Sample preparation and methods

The crystal studied was the 140 µm thick (010)-platelet from the Cr-bearing kyanite U-158 of Platonov *et al.* (1998), with a size of 870 x 220 µm and a chemical composition close to $(Al_{1.989}\ Cr_{0.014}\ Fe_{0.007}\ Ti_{0.001})_{\Sigma=2.011}\ [O/Si_{0.990}\ O_4]$. The specimen was thinned to about 30 µm thickness by grinding and then prepared by conventional ion-beam thinning (11° tilt angle, 6 kV, 1 mA). The procedures used were shown to not cause any electron damage under the applied experimental TEM conditions. This was done by treating a kyanite from Durango, Colorado, serving as standard in the TEM studies, in the same manner. Carbon coating prevented charging in the TEM.

TEM investigations were carried out using a Philips CM200 electron microscope with twin-lens configuration equipped with an EDAX X-ray analyser with an ultrathin window (0.3 µm thick, "Advanced Polymer") and a GATAN imaging filter (GIF). The microscope was operated at 200 kV. The electron source was a LaB_6 filament. The specimen was held by a Philips double tilt holder with Be-specimen cradle.

Most of the images were recorded using the GIF equipped with a CCD camera. Recording the images digitally requires short exposure times (0.5–1 s) with a defocused beam, thus reducing the electron current density on the specimen and preventing electron irradiation damage. Furthermore, recording the diffraction pattern with the CCD camera of the GIF has the advantage of yielding a significantly larger dynamic range compared with photographic recordings, so the very weak reflections alongside strong ones are visible in the CCD camera. Its disadvantage is the small entrance aperture of the GIF, so large images can be only obtained by combining several smaller images. All of the digitally recorded images were energy-filtered images using only the zero-loss peak of the electron energy spectrum by applying an energy window of about 5 eV, thus excluding the inelastically scattered electrons.

Chemical analysis was carried out in the scanning transmission mode (STEM) of the microscope using a nominal spot size of about 4 nm and a tilt angle of 20° of the specimen towards the detector. The probe current was 0.2 nA. Counting time was 200 s, resulting in an analytical error due to counting statistics of about 5-8 % rel. for Al, 7-9 % rel. for Si and up to 50 % rel. for Cr and Fe. The k_{AB}-factors necessary for quantitative analysis were calculated using the EDAX software package based on the electron microprobe analyses of the same specimen. The specimen thickness necessary for absorption correction was determined by electron energy-loss spectroscopy EELS using the total intensity of the electrons reaching the spectrometer and the intensity of the zero-loss peak (see Egerton, 1996). The specimen thickness is given by the expression $t = \lambda * \ln (I_t/I_o)$ with I_t the total intensity, I_o the intensity of the zero-loss peak, and λ the mean free path of the electrons in the specimen. The mean free path of 200 kV electrons in kyanite was estimated at about 120 nm using the methods of Egerton (1996) and Malis *et al*. (1988). The quantitative results were normalized to 100 % by the EDAX sofware.

Elemental mapping of aluminium and silicon was performed with the Al-L_3 edge and the Si-L_3 edge using the three-window method. Two pre-edge images were used for modelling the background. The method is described in Reimer (1995) and Egerton (1996).

Results and their evaluation

Fig. 1 presents a TEM bright-field (Fig. 1a) and a dark-field image (Fig. 1b) of the (010)-plate of kyanite as well as the corresponding diffraction pattern with zone axis $[110]_{ky}$ (Fig. 1c). Characteristic features of the bright-field image are tiny dark contrasts with a typical size of 5–10 nm. Many of these exhibit a typical "coffee bean" contrast as visible in Fig. 1a, with the contrast-free zone in the centre of the dark spots oriented E-W in the image of Fig. 1a. Such a type of contrast has been described from coherent precipitates, dislocation loops (Ashby & Brown, 1964a,b), and from irradiation defects (Martin *et al*., 1996). The intensity of the dark contrasting spots in the bright-field image depends on the orientation of the foil. The variation of intensity of the contrast with tilting suggests that it originates from diffraction contrast. The dark-field image of the same area was obtained using the $(\bar{2}24)_{ky}$ reflection (d = 0.133 nm) which are superimposed by $(12\bar{3}5)_{Al_2O_3}$ (d =

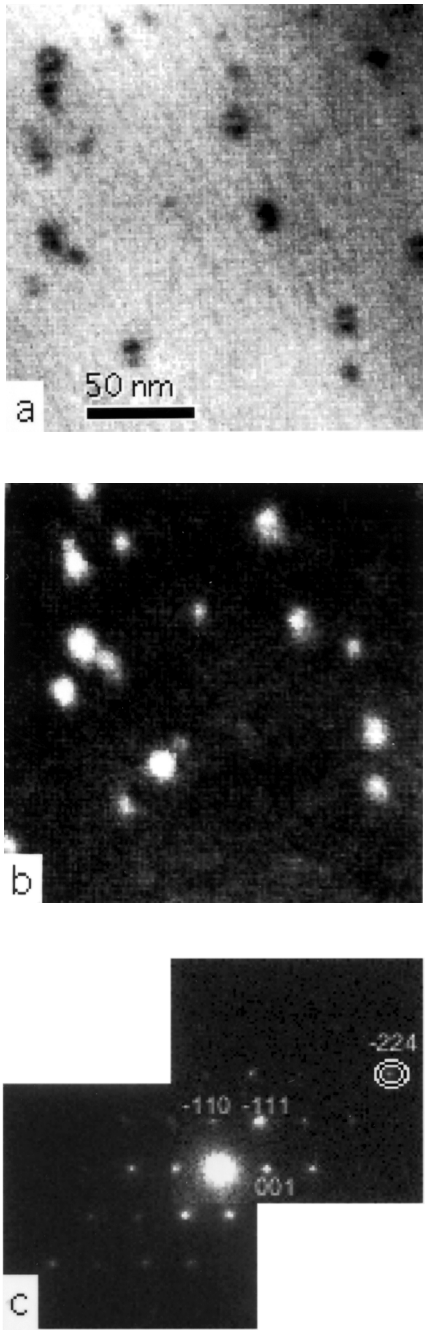

Fig. 1. The zero-loss filtered bright-field image in Fig. 1a shows dark contrasts with a line of no contrast in the centre; these are called coffee-bean contrasts. The corresponding dark-field image (Fig. 1b) using the reflection indicated by a circle in the diffraction pattern (Fig. 1c) exhibits the dark contrasts in the bright-field image as bright spots.

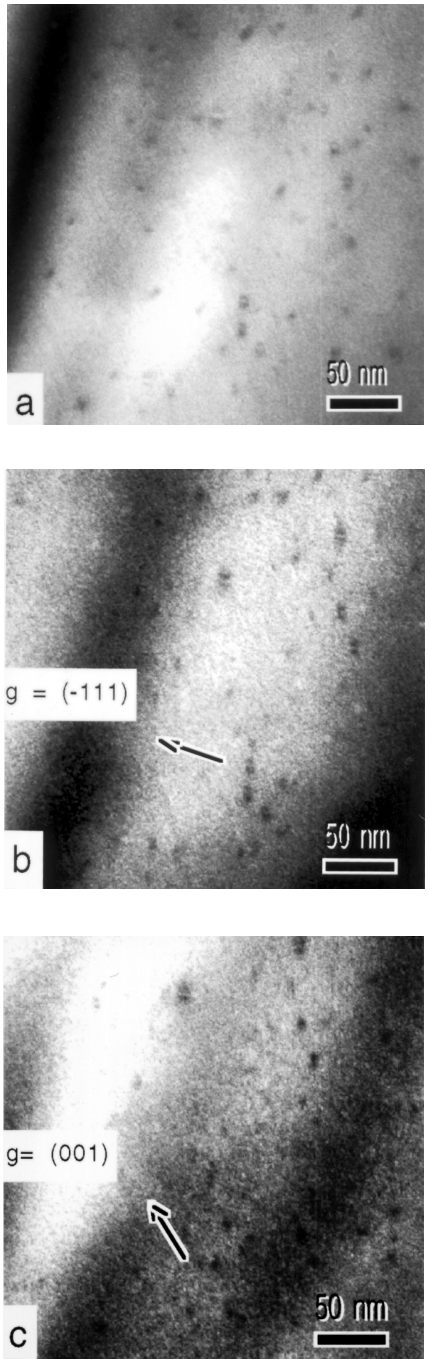

Fig. 2. Bright-field image of another part of the studied kyanite platelet (a) using the same zone axis as in Fig. 1 and two dark-field images of the same area using the kyanite $(\bar{1}11)$- or (001)- reflections (b) or (c), respectively. Note that the orientation of the line of no contrast does not change in either of the dark-field images.

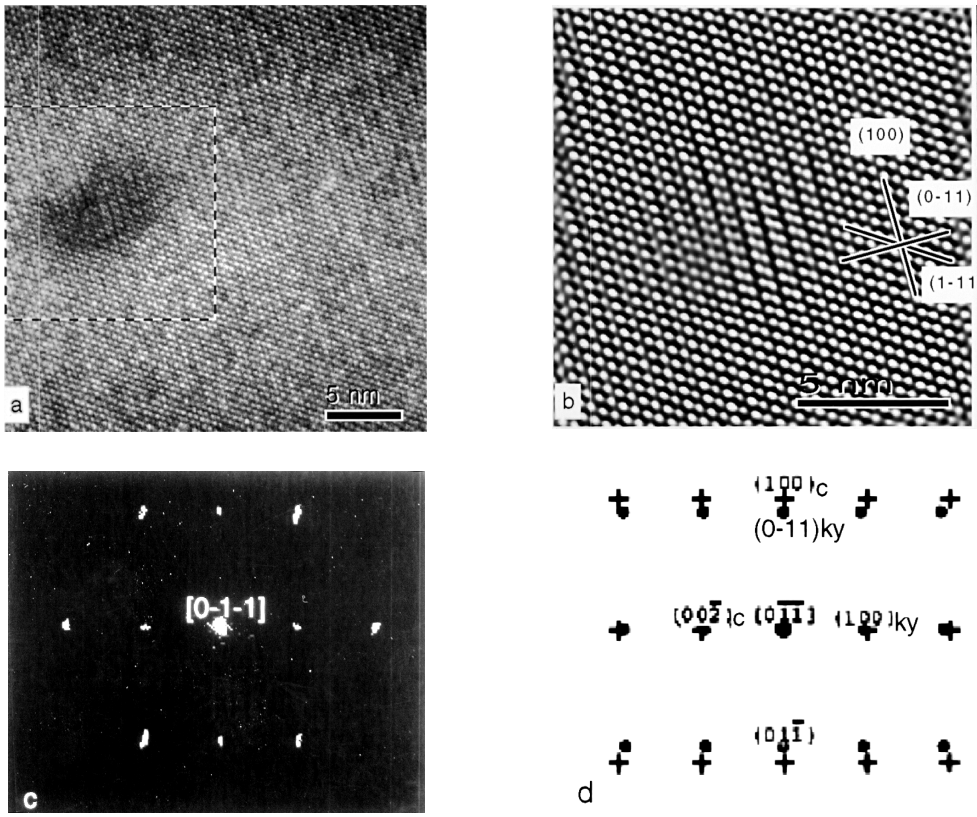

Fig. 3. High-resolution image of an area (a) with dark contrasts and zone axis $[0\bar{1}\bar{1}]_{ky}$, and (b) the corresponding enlarged Fourier filtered image of the area indicated in (a). When looking parallel to the (100) planes of kyanite, a slight distortion of the lattice fringes can be seen. (c) Experimental diffraction pattern (fast Fourier transform FFT) of the HREM image shown in (a) with split reflections. (d) Simulated diffraction pattern of kyanite with zone axis $[0\bar{1}\bar{1}]_{ky}$ and superimposed corundum lattice with zone axis $[0001]_{cor}$ assuming the lattice plane orientation relationship $(100)_{ky}$ // $(0001)_{cor}$. The simulated pattern is on the same scale; it shows the same splitting of reflections and fits the experimental FFT pattern very well (*cf.* Text).

0.133 nm) or $(03\bar{3}0)_{Al_2O_3}$ (d = 0.137 nm) when small amounts of an incipient unmixing corundum-type structure are present in the kyanite matrix. The observed intensity of the $(\bar{2}24)_{ky}$ reflection is much larger than the other reflections in its vicinity (Fig. 1c). This supports the suggestion that this reflection is formed by kyanite plus contributions from the Al_2O_3 -type volume elements. The dark-field image obtained using this reflection shows that the dark contrasts of the bright-field pattern (Fig. 1a) now appear as bright spots (Fig. 1b).

Fig. 2 presents two out of several dark-field images (Fig. 2b and c) acquired with different imaging vectors with the corresponding bright-field image shown on top (Fig. 2a). The zone axis used is [110]. The bright-field image shows many coffee bean contrasts. The contrast free zone of these is oriented approximately E-W. The two dark-field images show the same contrast with the same orientation of the contrast-free zone, as can be seen in the bright-field image. On the basis of the first criterion of Ashby & Brown, (1964a,b), it is possible to discriminate spherically symmetric strain fields from strain fields originating from plate-like inclusions on the basis of the behaviour of their varying imaging vectors. In the case of spheroidal inclusions, the line of no contrast is always perpendicular to the imaging vector $\vec{g}$. Therefore, the line of no contrast rotates with changing $\vec{g}$. However, in the case of plate-like inclusions, the line of contrast does not rotate with

changing imaging vector $\vec{g}$. Thus, it may be concluded that the coffee bean contrast observed here (Fig. 2) is caused by very small platelets included in the kyanite matrix, because, in this case, it is expected that the line of no contrast will be visible only under special imaging conditions ($\vec{g}*\Delta r \neq 0$). The observed width of the contrast-free zone indicates a platelet thickness of about 2 nm.

It was mentioned above that spots of dark contrast might originate from irradiation damage when examining kyanite with TEM, especially under focused beam conditions (Grobety & Veblen, 1995). Such effects are to be ruled out in the case of kyanite U-158 for the following reasons: (i) the kyanite was investigated using a defocused electron beam, thus keeping the probability of irradiation damage low. (ii) Our experience with phenomena related to electron irradiation damage in quartz shows that the features observed here differ greatly from such structural damage. (iii) Contrasts originating from irradiation damage show a noncrystalline centre (Hobbs *et al*., 1980; Martin *et al*., 1996). This was not observed in the case of U-158. (iv) Due to the Gaussian intensity distribution of the electron beam, the centre of an irradiated area always shows a high density of damage centres and a fading out of defect density towards the outer parts of the irradiated area. No such distribution of the dark contrasts was observed in U-158. (v) Irradiation experiments show an increasing number and size of damage centres on prolonged irradiation (Martin *et al*., 1996). No such effects were observed in U-158 under the imaging conditions used (condenser aperture 100 μm, spot size 200 nm, defocused beam). (vi) High-resolution images of irradiated areas in quartz show that the lattice fringes in the centre of a damaged area are replaced by an amorphous contrast, as typically observed with noncrystalline carbon (Pascucci *et al*., 1983; Inui *et al*., 1990). No such effects were observed in kyanite U-158. Instead, the high-resolution images presented here exhibit a change in the lattice fringe spacing, indicating very small amounts of platelet-like material in the kyanite matrix, which is structurally modified as shown below.

In conclusion: Kyanite U-158 contains incipient inclusions, irregularly distributed in the kyanite crystal, which form very small platelet-like volumes about 2 nm thick and typically 5-10 nm wide. This corroborates the hypothesis of a precursor for a chromium-bearing alumina-type exsolution in kyanite (Platonov *et al*., 1998). Further information may be gathered from checking the orientation relationship between the kyanite structure matrix and the inferred incipient alumina-type exsolution on the basis of the HRTEM study, and by attempting to obtain some results on the chemical composition of the exsolution precursor phase.

As regards the first aspect, Fig. 3 shows the results of HRTEM on areas with dark contrast. Fig. 3a represents the zero-loss filtered HRTEM image with $[0\bar{1}\bar{1}]$ zone axis. Fig. 3b shows a Fourier-filtered image of the area marked as a quadrangle in Fig. 3a using the reflections of the diffraction pattern (fast Fourier transform FFT) given in Fig. 3c. A slight lattice fringe distortion of the (100) fringes of kyanite is visible in Fig. 3b. Fig. 3d is a simulated diffraction pattern of kyanite superimposed onto corundum with the orientation relationship $[0\bar{1}\bar{1}]_{ky}$ // $[01\bar{1}0]_{cor}$ and $(100)_{ky}$ // $(0001)_{cor}$. Dots indicate the reflections of kyanite in Fig. 3d and crosses indicate the corundum reflections. Both diffraction patterns are on the same scale. The simulated diffraction pattern fits the experimental diffraction pattern quite well.

The agreement between simulated and experimental diffraction pattern supports the above orientation relationship, and suggests it is the correct basis for the observations. This means that the c-axis of the corundum-type lattice of the incipient exsolution is perpendicular to the (100) cleavage plane of kyanite. Grobety & Veblen (1995) found stacking faults parallel to this cleavage in kyanite. Simulations do not fit the observed diffraction patterns if we assume an orientation relationship in which the hexagonal close-packed oxygen layers of the corundum type lattice are parallel to the corresponding layers in the approximately cubic close-packed oxygen layers of the kyanite structure (Burnham, 1963), or any other additional orientation relationships.

As regards the second aspect mentioned above, it should be noted that the inelastically scattered electrons of the electron energy-loss spectrum (EELS) can be used for elemental mapping. This involves recording at least two images, one before and one after the ionisation edge. Another method is the three-window technique, which requires the acquisition of two images before the ionisation edge and one after the ionisation edge. These techniques are described in Reimer (1995) and Egerton (1996). Elemental mapping was performed on the kyanite specimen using the Al L_3 edge (73 eV) and the Si L_3 edge (100 eV). The corresponding K edges (Al K = 1560 eV; Si K = 1839 eV) were not used because this requires a high electron current density with long exposure times which would cause severe irradiation damage.

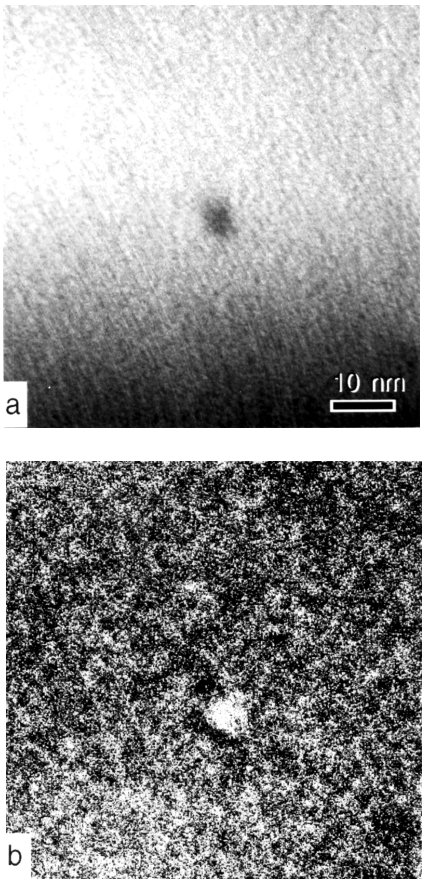

Fig. 4. Bright-field image showing a single area (a) of dark contrast and the corresponding Al-mapping (b) using the Al-L_3 ionisation edge showing the area of dark contrast to be aluminium enriched (*cf.* text).

Fig. 4a shows a zero-loss filtered bright-field image with a single dark contrast. An elemental map (Fig. 4b) of the same area using the Al-L_3 edge (three-window technique) exhibits a bright spot at the location of the dark spot in Fig. 4a, thus demonstrating Al-enrichment in the dark spot. The results of a similar experiment are shown in Fig. 5. Dark spots, some with coffee bean contrast are visible in the zero-loss filtered bright-field image in Fig. 5a. Some spots are indicated by arrows. An elemental map of Al is given in Fig. 5b. The spots indicated by arrows in the bright-field image appear now as bright spots in the Al map thus indicating a local increase of the Al concentration. The Si map exhibits dark spots at the locations of the dark contrasts in Fig. 5a according to a local decrease in the Si concentration. This observation

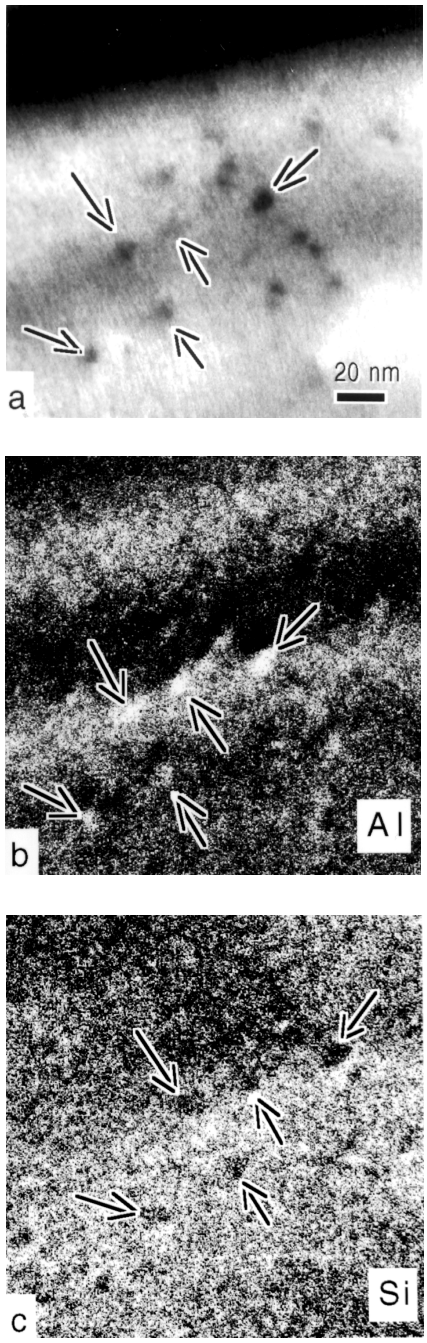

Fig. 5. (a) Bright-field image of another part of the kyanite (010) foil exhibiting numerous areas of dark contrast, some of them with coffee-bean shaped internal structure. All these are Al-enriched and concomitantly Si-depleted as demonstrated by the Al- and Si- elemental maps, (b) and (c), using the L_3-ionisation edges of these elements, (*cf.* text).

Table 1. Analytical results on two areas in the (010)-plate of kyanite U-158. Outside = analyses taken outside dark contrasts in the undisturbed kyanite matrix. Inside = analyses taken inside an area of dark contrast. Indicated spot size was 4 nm in diameter.

	Outside		Inside	
Number of analysis	7		10	
	wt.%	std.	wt.%	std.
Al_2O_3	59.93	(0.90)	62.3	(1.79)
Cr_2O_3	1.06	(0.22)	1.04	(0.15)
FeO	0.39	(0.09)	0.32	(0.10)
SiO_2	38.60	(0.70)	36.3	(1.64)

supports the hypothesis of very small incipient corundum-type exsolutions in the kyanite matrix.

EELS spectra of areas with dark contrast are identical to those of areas without dark contrasts. The beam diameter was 55 nm during acquisition and we might expect the volume of the inclusions to be too small to give a detectable signal in the EELS spectrum. The volume fraction of the inclusions was estimated from the images to be in the range 0.1–0.01vol. %. In relation to the volume of the whole crystal, the fraction is smaller because the distribution of the inclusions is inhomogeneous.

In an attempt to obtain qualitative information on the chemical composition of the dark contrasts, X-ray analysis was carried out in the STEM-mode using a spot size of 4 nm. Since it is clear that layers of the undisturbed kyanite matrix will exist above and/or below a dark contrast showing a chemical composition and structure different from kyanite, the properties of the matrix will definitely obscure those of the kyanite. In any case, the alumina concentration inside the dark spots should be slightly enhanced compared with the undisturbed matrix according to the results discussed above. The analytical results obtained inside and outside the dark spots (Table 1) show the former indeed to be more alumina–rich than the latter, in agreement with the results of elemental mapping (Fig. 4 and Fig. 5). As to be expected, the silica content varies inversely with alumina. The chromium- and iron concentrations are the same within the limits of error (Table 1).

Conclusions

TEM and HRTEM observations on the kyanite (010) crystal platelet U-158, as well as structural inferences from such observations, were combined with elemental mapping and attempts to obtain at least qualitative chemical information from X-ray analysis in the STEM mode. The results support the hypothesis explaining the results of electronic spectroscopy carried out on this mineral, namely, the presence of incipient alumina-type exsolution in the kyanite. This leads to crystal field properties for any incorporated Cr^{3+} that differ greatly from those of the kyanite structural matrix (Platonov *et al*., 1998). The exsolutions form very small platelike volumes about 2 nm thick and 5–10 nm wide, showing smooth interfaces with the matrix. The volume fraction of these incipient exsolutions, previously termed "precursors of exsolution" is less than 0.1 vol. %. The orientation relationship between the corundum-type exsolution precursor and the kyanite matrix is $[0\bar{1}\bar{1}]_{ky}$ // $[01\bar{1}0]_{cor}$ and $(100)_{ky}$ // $(0001)_{cor}$.

Acknowledgements: A.N.P. wishes to thank the Deutsche Forschungsgemeinschaft, Bonn-Bad Godesberg, for generously providing research stipends in 1998 and 1999. The financial support of INTAS under grant no. 97-32174 is also gratefully acknowledged.

References

Ashby, M.F. & Brown, L.M. (1964a): Diffraction contrast from spherically symmetrical coherency strains. *Phil. Mag*., **8**, 1083-1103.

– , – (1964b): On diffraction contrast from inclusions. *Phil. Mag*., **8**, 1649-1676.

Burnham, C.W. (1963): Refinement of the crystal structure of kyanite. *Z. Kristallogr*., **118**, 337-360.

Egerton, R.F. (1996): Electron energy-loss spectroscopy in the electron microscope. Plenum press, New York and London, p. 301-310. 2. Edition.

Grobety, B.H. & Veblen, D. (1995): HRTEM study of stacking faults and polytypism in kyanite. *Eur. J. Mineral*., **7**, 807-818.

Hobbs, L.W. & Pascucci, M.R. (1980): Radiolysis and defect structure in electron-irradiated alpha-quartz. *J. Phys.*, C6, **41**, 237-242.

Inui, H., Mori, H., Sakata, T., Fujita, H. (1990): Electron irradiation induced crystalline to amorphous transition in quartz single crystals. *J. of Non-Crystalline Solids*, **116**, 1-15.

Malis, T., Cheng, S.C., Egerton, R.F. (1988): EELS log-ratio technique for specimen-thickness measurement in the TEM. *J. Electron Microscope Technique*, **8**,193-200.

Martin, B., Flörke, O.W., Kainka, E., Wirth, R. (1996): Electron irradiation damage in quartz. *Phys. Chem. Minerals*, **23**, 409-417.

Pascucci, M.R., Hutchison, J.L., Hobbs, L.W. (1983): The metamict transformation in alpha-quartz. *Radiation Effects*, **74**, 219-226.

Platonov, A.N., Tarashchan, A.N., Langer, K., Andrut, M., Partzsch, G., Matsyuk, S.S. (1998): Electronic absorption and luminescence spectroscopic studies of kyanite single crystals: differentiation between excitation of FeTi charge transfer and Cr^{3+} dd transitions. *Phys. Chem. Minerals*, **25**, 203-221.

Reimer, L. (1995): Electron spectroscopic imaging. *In*: Energy-filtering transmission electron microscopy. L. Reimer (ed.) Springer Series in Optical Sciences **71**, Springer Verlag Berlin Heidelberg.

Winter, J.K. & Ghose, S. (1979): Thermal expansion and high-temperature crystal chemistry of Al_2SiO_5 polymorphs. *Am. Mineral*., **64**, 573-586.

Received 10 January 2000
Modified version received 16 July 2000
Accepted 6 November 2000